Supplementary Material: Entanglement Spheres and a UV-IR connection in Effective Field Theories

Natalie Klco[1,*] and Martin J. Savage[2,†]

[1] *Institute for Quantum Information and Matter (IQIM) and Walter Burke Institute for Theoretical Physics, California Institute of Technology, Pasadena CA 91125*

[2] *InQubator for Quantum Simulation (IQuS), Department of Physics, University of Washington, Seattle, WA 98195*

S1. LATTICE CORRELATION FUNCTIONS IN THE THERMODYNAMIC LIMIT

For free scalar fields, two-point correlation functions define the information content in the field. In this appendix, formulations of these expectation values are presented in the thermodynamic limit of large lattices with a form conducive to computation. In 1D and 2D, analytic expressions are provided, while in higher dimensions, a one dimensional integral is provided with convergence that improves with increasing dimension. For $D \geq 2$, correlation functions are IR convergent, allowing the mass to be reliably set to zero.

For arbitrary D, the two-point lattice field correlation function with unit lattice spacing and field separation described by a vector of positive integers, $\mathbf{n}$, is

$$\langle \phi(0)\phi(\mathbf{n})\rangle = G(\mathbf{n}) = \sum_p \frac{e^{i\mathbf{p}\cdot\mathbf{n}}}{2L^D} \frac{1}{\sqrt{m^2 + 4\sum_i \sin^2\left(\frac{p_i}{2}\right)}} \quad , \tag{S1}$$

for $p_i \in \frac{2\pi}{L}\mathbb{Z}_L$ with $\mathbb{Z}_L$ the set of integers between 0 and $(L-1)$. In the thermodynamic limit ($L \to \infty$),

$$G(\mathbf{n}) = \frac{1}{2\pi^D} \int_0^\pi \mathrm{d}^D p \ \frac{\prod_i \cos(p_i n_i)}{\sqrt{m^2 + 4\sum_i \sin^2\left(\frac{p_i}{2}\right)}} \quad , \tag{S2}$$

with $\mathrm{d}^d p = \prod_i \mathrm{d}p_i$. A Gaussian integral may be introduced to capture the radical in the denominator

$$G(\mathbf{n}) = \frac{1}{2\pi^D} \int_0^\pi \mathrm{d}^D p \ \prod_i \cos(p_i n_i) \left[\frac{2}{\sqrt{\pi}} \int_0^\infty \mathrm{d}x \ e^{-(m^2+2D)x^2} e^{\sum_i (2\cos p_i)x^2}\right] \quad . \tag{S3}$$

The integral representation of the modified Bessel function of the first kind may subsequently be identified to yield,

$$G(\mathbf{n}) = \frac{1}{\sqrt{\pi}} \int_0^\infty \mathrm{d}x \ e^{-(m^2+2D)x^2} \prod_i I_{n_i}(2x^2) \quad , \tag{S4}$$

where, for integer order, the modified Bessel function may be expressed as,

$$I_\alpha(z) = \frac{1}{\pi} \int_0^\pi \mathrm{d}\theta \ e^{z\cos\theta} \cos\alpha\theta \quad . \tag{S5}$$

The resulting expression for the two-point correlation function is a single integral for any D. As $I_\alpha(z) \sim e^z/\sqrt{2\pi z}$ for large arguments, the convergence of these integrals improves with increasing D.

Employing similar procedures for the two-point functions of conjugate momentum field operators yields analogous computationally advantageous expressions. In the thermodynamic limit with massless fields, the expectation value may be written as,

$$\langle \pi(0)\pi(\mathbf{n})\rangle \equiv H(\mathbf{n}) \tag{S6}$$

* natklco@caltech.edu

† On leave from the Institute for Nuclear Theory; mjs5@uw.edu

$$= \frac{1}{2\pi^D}\int_0^\pi \mathrm{d}^D p\ \prod_i \cos(p_i n_i)\sqrt{m^2+4\sum_i \sin^2\left(\frac{p_i}{2}\right)} \tag{S7}$$

$$= \frac{1}{2\pi^D}\int_0^\pi \mathrm{d}^D p\ \frac{\prod_i \cos(p_i n_i)}{\sqrt{m^2+4\sum_i \sin^2\left(\frac{p_i}{2}\right)}}\left(m^2+2D-2\sum_j \cos(p_j)\right) \quad . \tag{S8}$$

Associating the additional $\cos(p_i)$ factors with a partial derivative of the modified Bessel function, Eq. (S5), with respect to its argument, the correlator becomes

$$H(\mathbf{n}) = \int_0^\infty \frac{e^{-(m^2+2D)x^2}}{\sqrt{\pi}}\left((m^2+2D)\prod_i I_{n_i}(2x^2) - 2\sum_j \frac{\partial_j}{\partial(2x^2)}\prod_i I_{n_i}(2x^2)\right) \quad , \tag{S9}$$

where $\frac{\partial_j}{\partial(2x^2)}$ indicates the argument derivative of the Bessel function associated with the j^{th} lattice direction. Given that this is expressible as the average of the Bessel functions of neighboring order,

$$\partial_z I_\alpha(z) = \frac{I_{\alpha-1}(z)+I_{\alpha+1}(z)}{2} \quad , \tag{S10}$$

$H(\mathbf{n})$ can be written as a linear combination of field correlators,

$$\begin{aligned} H(\mathbf{n}) &= (m^2+2D)G(\mathbf{n}) - \sum_{\{\mathbf{n}'\}} G(\mathbf{n}') \quad , \\ &\to m^2 G(\mathbf{n}) - \nabla^2 G(\mathbf{n}) \ , \end{aligned} \tag{S11}$$

where the set $\{\mathbf{n}'\}$ is the set of 2D integer vectors shifted by ± 1 in each possible direction of the D dimensional lattice. Thus, the numerical stability of the field correlators extends to correlators in conjugate momentum space.

A. One Spatial Dimension

The integral expression of Eq. (S4) in 1D can be evaluated in closed form as,

$$G(n) = \frac{1}{2\sqrt{\pi}(2+m^2)^{n+1/2}}\Gamma\left[\frac{1}{2}+n\right]\ {}_2\tilde{F}_1\left(\begin{matrix}\frac{1+2n}{4},\frac{3+2n}{4}\\ 1+n\end{matrix};\frac{4}{(2+m^2)^2}\right) \quad , \tag{S12}$$

where ${}_2\tilde{F}_1\left(\begin{matrix}a,b\\ c\end{matrix};z\right) = {}_2F_1\left(\begin{matrix}a,b\\ c\end{matrix};z\right)/\Gamma(c)$ is the regularized hypergeometric function, consistent with e.g., Ref. [26]. The ${}_2F_1$ function is finite for finite values of its parametric arguments and for $|z|<1$. Thus, the mass in 1D is a necessary IR regulator that must be maintained nonzero throughout calculations.

B. Two Spatial Dimensions

In 2D, the field correlators can be solved analytically, a valuable capability for the finely-pixelated wavefunctions presented in Fig. 2 of the main text. Using the following identity for the product of two modified Bessel functions of equal argument [80, Eq. 10.31.3], the two point function of Eq. (S4) becomes,

$$G(n_x,n_y) = \frac{1}{\sqrt{\pi}}\int_0^\infty \mathrm{d}x\ e^{-(m^2+4)x^2}x^{2(n_x+n_y)}\sum_{k=0}^\infty \frac{(n_x+n_y+k+1)_k\, x^{4k}}{k!\Gamma(n_x+k+1)\Gamma(n_y+k+1)} \quad , \tag{S13}$$

relying on the closure of a product of ${}_0F_1$ functions into a ${}_2F_3$ generalized hypergeometric function. The x integral is calculated as a Gaussian moment,

$$G(n_x,n_y) = \frac{1}{2(4+m^2)^{\frac{1+2n_x+2n_y}{2}}\sqrt{\pi}}\sum_{k=0}^\infty \frac{(n_x+n_y+k+1)_k}{k!\Gamma(n_x+k+1)\Gamma(n_y+k+1)}\frac{\Gamma\left(\frac{1}{2}+2k+n_x+n_y\right)}{(4+m^2)^{2k}} \quad . \tag{S14}$$

Using the Legendre duplication relation of the Gamma function and the associated Pochhammer identity,

$$\left(\frac{z}{2}\right)_n \left(\frac{z}{2}+\frac{1}{2}\right)_n = 2^{-2n}(z)_{2n} \quad , \quad \frac{\left(\frac{a+b+1}{2}\right)_k \left(\frac{a+b+2}{2}\right)_k}{(a+b+1)_k} \;=\; 4^{-k}(1+a+b+k)_k \quad , \tag{S15}$$

a generalized hypergeometric function can be identified for the two-point correlation function,

$$G(n_x,n_y) = \frac{1}{2\sqrt{\pi}(4+m^2)^{1/2+n_x+n_y}} \frac{\Gamma\left(\frac{1}{2}+n_x+n_y\right)}{\Gamma(n_x+1)\Gamma(n_y+1)} \times {}_4F_3\left(\begin{matrix}\frac{n_x+n_y+1}{2}, \frac{n_x+n_y+2}{2}, \frac{n_x+n_y}{2}+\frac{1}{4}, \frac{n_x+n_y}{2}+\frac{3}{4} \\ 1+n_x, 1+n_y, 1+n_x+n_y\end{matrix}; \frac{16}{(4+m^2)^2}\right) \quad , \tag{S16}$$

where

$${}_pF_q\left(\begin{matrix}a_1,\cdots,a_p \\ b_1,\cdots,b_q\end{matrix}; z\right) \equiv \sum_{k=0}^{\infty} \frac{z^k}{k!} \frac{\prod_{j=1}^{p}(a_j)_k}{\prod_{\ell=1}^{q}(b_\ell)_k} \quad . \tag{S17}$$

In the massless limit, the argument of the hypergeometric function becomes unity. Because the $|z|=1$ case is finite and well defined for ${}_4F_3\left(\begin{matrix}a_1,a_2,a_3,a_4 \\ b_1,b_2,b_3\end{matrix}; z\right)$ if $\sum_j b_j - \sum_j a_j > 0$ (which will always be satisfied above), the mass does not need to be retained as an explicit IR regulator. The correlators of conjugate momentum operators are related through Eq. (S11) as,

$$H(n_x,n_y) \;=\; (4+m^2)G(n_x,n_y) - G(n_x-1,n_y) - G(n_x+1,n_y) - G(n_x,n_y-1) - G(n_x,n_y+1) \quad . \tag{S18}$$

It is expected that analytic expressions exist for the field correlators in higher dimension, $D>2$, though their form remains elusive. For 3D, it has been computationally practical (leveraging the mentioned improving convergence in higher dimensions) to calculate the lattice two-point functions numerically through a truncated expansion of modified Bessel functions in Eq. (S4).

S2. LOGARITHMIC NEGATIVITY, GAUSSIAN SEPARABILITY CRITERIA AND THE ENTANGLEMENT SPHERE

While logarithmic negativity can be difficult to interpret as an entanglement measure in general, its current application, combined with the separability criterion of Ref. [47] and the distillation criterion of Ref. [79], has yielded a uniquely informative quantification of quantum correlations in the free lattice scalar field theory vacuum. Generically, negativity has been connected to the operational measure of *distillable entanglement* i.e., the population of entangled pairs that can be asymptotically extracted from an ensemble of the state through local interactions [49]. Thus, the negativity will inform the spacelike entanglement that could be extracted by locally interacting detectors.

As an upper bound to the distillable entanglement, a vanishing logarithmic negativity between regions of a field indicates that two sensors/detectors interacting at spacelike separations with the field would never themselves become entangled, even if the local regions of the field are expressed with a single non-separable quantum wavefunction. The latter extension indicates that a vanishing negativity is generically inconclusive with respect to the separability of the regions (e.g., due to the possibility of bound entanglement [54]). Non-zero negativity, however, is conclusive with respect to inseparability. Because negativity quantifies the physical validity of a density matrix after transformation by a particular local positive map (partial transposition), any violation of physicality heralds the presence of entanglement. However, as an upper bound, a non-zero negativity generically carries no conclusive information about the operational entanglement structure of the field.

For the specific application to Gaussian states representing the free scalar vacuum, both vanishing and non-vanishing negativity calculations become more informative. As such, the free scalar vacuum is a special case, distinct but reminiscent of e.g., the $(1\times N)$-mode or bisymmetric Gaussian states for which the negativity is known to be a

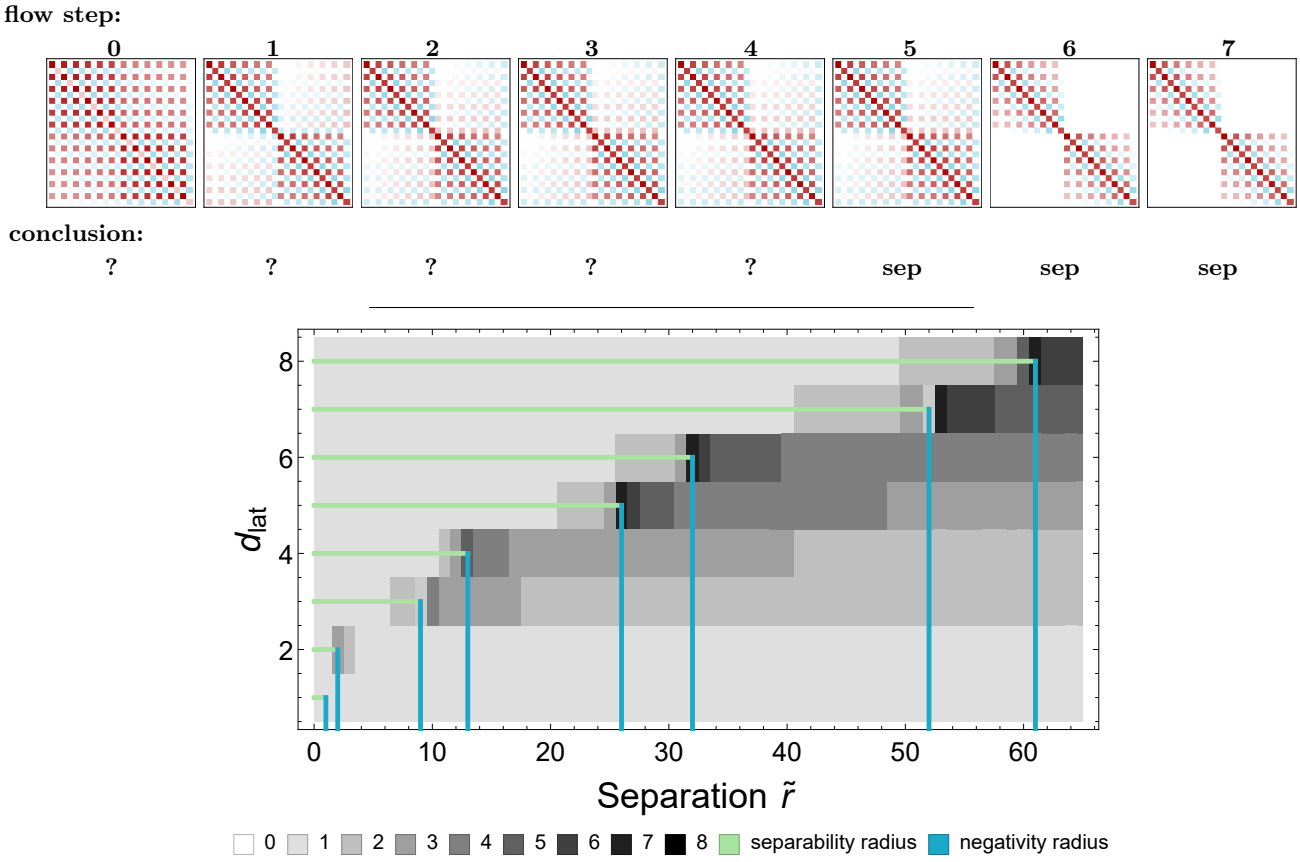

FIG. S1. (Upper panel) Steps in the covariance matrix flow arising from two regions of 1D lattice scalar field theory vacuum with $d_{\text{lat}} = 6$ for a representative separation with $\tilde{r} = 34$ outside the separability sphere, as defined in Eq. (S19). (Lower panel) The separability and negativity radii are shown to coincide for a range of d_{lat}.

necessary and sufficient condition for entanglement. For Gaussian states, if a bipartite system is found to have non-zero negativity (NPT), then non-zero distillable entanglement is determined to be present [79].

To further analyze the systems beyond the negativity sphere with vanishing negativity (positive partial transpose, PPT), the entanglement criterion of Ref. [47] can be profitably employed. A "flow" for the vacuum state covariance matrix, σ, was designed of the following form

$$\sigma_0 = \begin{pmatrix} A_0 & C_0 \\ C_0^T & B_0 \end{pmatrix} \quad , \qquad \sigma_{N+1} = \begin{pmatrix} A_N - \text{Re}(X_N) & -\text{Im}\,(X_N) \\ -\text{Im}\,(X_N^T) & A_N - \text{Re}(X_N) \end{pmatrix} \quad , \tag{S19}$$

with $X_N = C_N(B_N - i\Omega)^{-1}C_N^T$ inspired by the Schur complement's relation to the matrix positivity condition. For the N continuous variable modes of the field, $i\Omega = [\hat{\mathbf{r}}, \hat{\mathbf{r}}^T]$ is the matrix of canonical commutation relations incorporating the uncertainty principle into the symplectic language with $\hat{\mathbf{r}}$ the $2N$ dimensional vector of $\hat{\phi}_i, \hat{\pi}_i$ canonical operators. It is shown in Ref. [47] that this non-linear map preserves the separability of states, flowing (in)separable states to (in)separable states. In addition to this preservation, the flow is demonstrated to transform covariance matrices into forms for which the separability criterion can be more readily determined by calculating e.g., the physicality of the reduced covariance matrix of the first region, A_N, indicating inseparability if A_N fails to pass the uncertainty principle requirements of $\sigma_{\text{phys}} - i\Omega \geq 0$. While the two criteria used to "detect" separability or inseparability of σ are commonly inconclusive when applied to covariance matrices, a few steps of the separability-preserving flow in practice produce a σ_N whose separability condition can be conclusively determined, and thus that of σ_0 determined by extension.

For example, consider the case of 6-site field regions ($d_{\text{lat}} = 6$) in 1D of the massless non-interacting lattice scalar

field. As previously calculated (e.g., Ref. [53]) the first lattice separation at which the negativity vanishes for this system, defining the negativity radius, is $\tilde{r}_{\mathcal{N}} = 32$. Inside this radius, the non-zero negativity indicates inseparability, but at and outside this separation, the vanishing negativity does not inform the separability of the field regions. Employing the separability-preserving non-linear map [47] in Eq. (S19) for a representative separation outside the negativity sphere of $\tilde{r} = 34$ produces the covariance matrix flow shown at the top of Fig. S1. The initial covariance matrix at flow step 0, written in the basis $\hat{\mathbf{r}} = \{\hat{\phi}_0, \hat{\pi}_0, \hat{\phi}_1, \hat{\pi}_1, \cdots, \hat{\phi}_5, \hat{\pi}_5\}$, is inconclusive with regard to the separability and inseparability criteria. However, after 5 flow steps, the covariance matrix σ_5 is determined to be separable. In this case, the flow arrives at the clearly separable fixed point in which the off-diagonal covariance matrix elements between regions vanish, though the criterion is capable of identifying separability prior to this point. The separability of σ_5 implies (by design) also the separability of σ_0, indicating that the vanishing negativity in this example is the result of a stronger condition that the two regions of the field are separable.

Exploring further this flow and the relationship between negativity and separability in the lattice scalar field ground state, the lower panel of Fig. S1 shows a gray-scale distribution of the number of flow steps necessary to conclusively determine separability. It can be clearly seen that the number of flow steps necessary to determine separability/inseparability is maximized along the surface of the negativity sphere. Unfortunately, the correlation matrices explored throughout the flow evolution become poorly conditioned at increased pixelations, requiring careful control of numerical precision even far from the continuum. Furthermore, Fig. S1 shows that the negativity radii (vertical blue lines), as calculated from Ref. [53] for each d_{lat} indicated by the line's height, exactly agree with the separability radii (length of horizontal green lines), determined by flowing each covariance matrix of region diameter d_{lat} and lattice region separation $\tilde{r}$. As discussed in the main text, this comparison indicates that the free lattice scalar field theory vacuum is a non-generic quantum state for which vanishing negativity is coincident with separability. The resulting promotion of the *negativity sphere* to an *entanglement sphere* emphasizes that negativity serves, in this case, as a clear quantifier of experimentally relevant quantum correlations. Spacelike separated detectors interacting locally with the vacuum at regions carrying zero/non-zero negativity will never/always be able to extract, in principle, entanglement from the vacuum.

S3. NUMERICAL CALCULATION OF β_{3D} AND γ_{3D}

In this appendix we elaborate on our calculation of the negativity between two pixelated spherical regions of massless noninteracting lattice scalar field theory in 3D, in particular the values of $\beta_{3D} = 7.6(1)$ and $\gamma_{3D} = 0.43(2)$, which are first calculations of these quantities. In general, the calculation follows the same procedure that led to the determinations of $\beta_{1D,2D}$ and $\gamma_{1D,2D}$ presented in previous works, but there are slight differences. The geometry of the calculation is that of two equal sized, approximately spherical pixelated regions of the lattice defining the two regions, A and B, that are separated along one of the Cartesian directions. Each region has a diameter along an axis defined by d_{lat} lattice sites and of length $(d_{\text{lat}} - 1)a$, and are separated by a surface-to-surface distance of $(\tilde{r} + 1)a$ and a distance between centers of $ra = (\tilde{r} + d_{\text{lat}} - 1)a$ lattice sites. (d_{lat} even or odd are both legitimate choices at finite lattice spacing that will produce the same continuum limit.)

Transverse dimensions are distinguished from the displacement direction. While calculations of negativity can proceed by the computation of two-point correlation functions followed by direct matrix diagonalization, the dimensionality of the problem in higher dimensions and the condition number of the matrix (from the polynomial scaling correlators giving rise to an exponentially decreasing negativity), motivate utilizing the discrete symmetries of the system from the outset. These include parity, reflections in the displacement plane and hypercubic symmetries. Due to their observed dominant contribution to the negativity, we form the A_1^+ irreps of the transverse H(D-1) group, defined by their radius from the transverse symmetry axis (including multiplicities where appropriate) for each distance along the displacement axis. These coordinates are used to construct the $\hat{G}$ and $\hat{H}$ matrices. For a given configuration, the calculation proceeds as follows:

1. define the lattice sites in regions A and B,

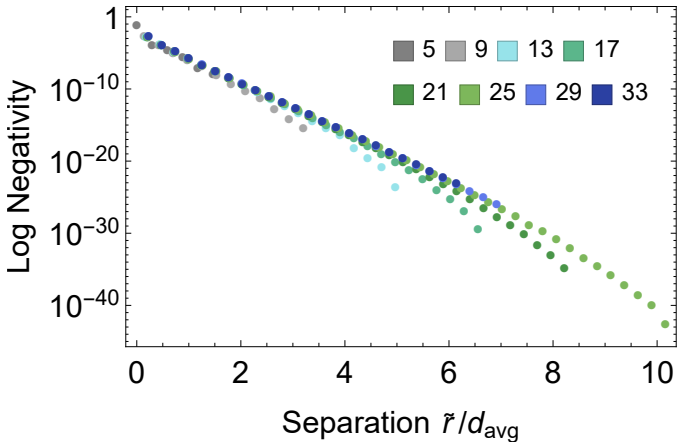

$1/d_{\text{lat}}$	$\beta_{3D}(d)$
0.030	7.6901(89)
0.034	7.735(15)
0.040	7.732(15)
0.048	8.014(65)
0.059	8.38(11)
0.077	9.70(16)
0.111	10.01(19)

FIG. S2. (Left) The calculated log negativity for different pixelations of 3D spheres. The values are provided in Table S1. (Right) The values of $\beta_{3D}^{(\text{eff})}$ determined for each pixelation, with the extrapolation to $1/d \to 0$ defining the continuum limit.

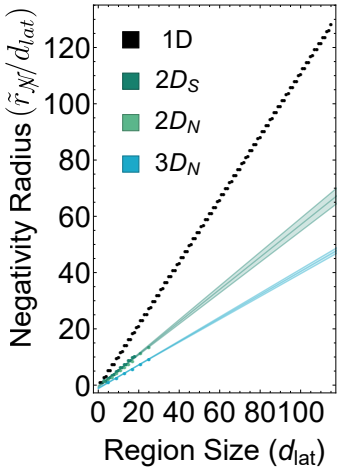

d_{lat}	$\tilde{r}_{\mathcal{N}}/d_{\text{avg}}$	$\tilde{r}_{\mathcal{N}}/d_{\text{lat}}$
5	1.46	1.0
9	$3.20^{(+0.14)}$	$2.56^{(+0.11)}$
13	$4.97^{(+0.18)}$	$4.31^{(+0.15)}$
17	$6.55^{(+0.2)}$	$5.83^{(+0.18)}$
21	$8.21^{(+0.21)}$	$7.57^{(+0.19)}$
25	$10.16^{(+0.22)}$	$9.32^{(+0.2)}$

FIG. S3. (Left) The log negativity radius as a function of pixelation in 1D, 2D and 3D. The slopes provide $\gamma_{1D,2D,3D}$. The results shown for 1D and 2D are those from Ref. [53]. (Right) Numerical locations of the last calculated non-zero negativity at the entanglement sphere. The uncertainties express the inexact determination of $\tilde{r}_{\mathcal{N}}$ with the chosen separation sample density.

2. determine the displacement vectors for each pair of A_1^+ in the system for a given longitudinal displacement,

3. numerically evaluate the integrals $G(\mathbf{n})$ and $H^\Gamma(\mathbf{n})$ (in the text) or retrieve the stored values, and form the appropriate symmetry combination,

4. multiply $\hat{G}$ and $\hat{H}^\Gamma$, and find the negative eigenvalues.

The calculations that we present here were performed using a combination of `Mathematica` and `Matlab`, due to their different optimizations for the combinations of analytic and numeric functions we have employed. In order to move beyond the calculations we show, more robust and scalable codes optimized for large-scale parallel computing will be required. The results of our calculations in 3D are provided in Table S1 and displayed in Fig. S2.

Leveraging techniques widely-used in the analysis of lattice QCD calculations, an effective mass is generated for each point in each of the sets of results given in Table S1. The effective masses tend to a constant from both small and large displacements, with a range that increases and oscillatory contributions that diminish with denser pixelation of the spheres. These effective masses lend themselves to Fourier transformation to extract the asymptotic constant with an associated uncertainty (the argument of the purely exponential behavior of the negativity) for each level of pixelation. The results of this extraction are presented in the table at the right of Fig. S2. For coarse pixelation, the range of

non-vanishing negativity that we have computed is sufficiently limited that a robust estimate of the systematic errors are not practical, and we have been able to compute only three reliable values of the argument of the exponential that can be used to extrapolate to the continuum with confidence. A linear extrapolation of the three results in Fig. S2 with the smallest values of $1/d$ yields $\beta_{3D} = 7.6(1)$. A higher precision result will require additional calculations at finer pixelation, which will enable extrapolations using higher-order polynomials. The present calculations, unlike our results in 2D, are the minimum that can be performed to obtain an extrapolated value.

The values of the points of vanishing negativity as a function of pixelation determine the coefficient γ_{3D}. The results shown in Table S1 of the negativity as a function of separation furnish the results given in the table at the right of Fig. S3 for the (dimensionless) point of vanishing negativity. Extracting the slope of these results with respect to $d_{\rm lat}$ yields a value of $\gamma_{3D} = 0.43(2)$. It is interesting that the suppression of fluctuations in higher dimension has allowed the precision attained in 3D to be commensurate with that attained in 2D. These numerical calculations provide early insight into the dependence of the vacuum entanglement structure on the spatial dimension of the field, yielding results sufficiently intriguing to motivate future calculations with higher precision and in higher dimension.

S4. DISPERSION RELATION IMPROVEMENT IN ONE DIMENSION

The numerical lattice scalar field theory calculations performed in this work, and the results of previously published works (e.g., Refs. [17, 53]), have employed the simplest discretization of the lattice energy-momentum relation in which the continuum momentum operator is approximated by a nearest neighbor finite-difference operation on lattice sites. It is helpful to quantify the sensitivity of the physics results we have presented in this paper to the choice of lattice discretization of this gradient operator. It is well known how to systematically improve the dispersion relation by introducing higher order operators, suppressed by positive powers of the lattice spacing, to remove higher-order contributions in momentum and to converge toward the desired $E^2 = k^2 + m^2$ of special relativity. However, for a finite number of lattice sites, only a finite number of independent finite-difference operators may be constructed, and each order of improvement corresponds to further smearing of the gradient operator over an increasing region of the lattice. To explore the impact of the discretization, we compare results in one dimension obtained with lattice dispersion relations of the form:

$$\begin{aligned} m^2 + 4\sin^2(k/2) \;&\rightarrow\; m^2 + k^2 - \frac{k^4}{12} + \frac{k^6}{360} - \frac{k^8}{20160} + \mathcal{O}\left(k^{10}\right) \\ m^2 + 4\sin^2(k/2) + \frac{4}{3}\sin^4(k/2) \;&\rightarrow\; m^2 + k^2 - \frac{k^6}{90} + \frac{k^8}{1008} + \mathcal{O}\left(k^{10}\right) \quad , \end{aligned} \tag{S20}$$

which have the same low-momentum behavior up to polynomial corrections and differ by $\mathcal{O}(1)$ at the edge of the Brillouin zone. These correspond to different discretizations while preserving the infrared behavior of the lattice scalar field theory, and correspond to leading order and $\mathcal{O}(k^4)$-improved lattice actions for the non-interacting lattice theory. While it might be tempting to consider the full dispersion relation directly, with the finite number of lattice sites in the system such an operator cannot be accurately obtained from a finite number of finite-difference operators. Different discretizations of the scalar field that preserve the energy-momentum relation correspond to including smearings of the gradient operator, and can be included as higher-order terms in the dispersion relation. As the goal of this Appendix is to illustrate the impact of modified UV physics on the entanglement structure of the field and because modified lattice actions are closely related to smearing for bosonic fields, the first order improvement of the dispersion relation is chosen to favor the relative impact of the UV modification.

In this Appendix, the negativity between two vacuum regions is calculated through two-point functions in which the naïve lattice dispersion relations (see Appendix S1), are replaced by the k^4-improved relations in Eq. (S20). Numerical evaluations of the correlation functions become increasingly weighted to low momentum at large distances, with the higher-order improvements making a decreasing contribution to each of the integrals. On the other hand, the long-distance negativity becomes increasingly sensitive to the short-distance behavior of the two-point functions and does explicitly probe these higher-order improvements, consistent with the main thesis of this article. Together, these observations indicate the presence of large cancelations between polynomially- and logarithmically-varying

$\bar{r}/d_{\rm avg}$	$\mathcal{N}$
$d_{\rm lat} = 5$	
0	1.19×10^{-1}
2.93×10^{-1}	2.00×10^{-4}
5.86×10^{-1}	3.97×10^{-5}
8.79×10^{-1}	4.31×10^{-6}
1.17	1.03×10^{-7}
1.46	1.64×10^{-8}
$d_{\rm lat} = 9$	
1.39×10^{-1}	2.88×10^{-3}
4.17×10^{-1}	1.90×10^{-4}
6.96×10^{-1}	1.32×10^{-5}
9.74×10^{-1}	1.70×10^{-6}
1.25	2.19×10^{-7}
1.53	1.37×10^{-8}
1.81	6.45×10^{-10}
2.09	8.72×10^{-11}
2.37	7.48×10^{-12}
2.64	2.51×10^{-13}
2.92	9.87×10^{-15}
3.2	6.30×10^{-16}
$d_{\rm lat} = 13$	
1.77×10^{-1}	2.44×10^{-3}
4.44×10^{-1}	2.43×10^{-4}
7.1×10^{-1}	1.93×10^{-5}
9.76×10^{-1}	2.91×10^{-6}
1.24	2.94×10^{-7}
1.51	3.84×10^{-8}
1.77	5.32×10^{-9}
2.04	5.33×10^{-10}
2.31	5.64×10^{-11}
2.57	6.60×10^{-12}
2.84	7.06×10^{-13}
3.11	6.16×10^{-14}
3.37	4.67×10^{-15}
3.64	5.82×10^{-16}
3.9	5.43×10^{-17}
4.17	1.05×10^{-18}
4.44	4.08×10^{-20}
4.7	1.90×10^{-21}
4.97	3.55×10^{-24}

$\bar{r}/d_{\rm avg}$	$\mathcal{N}$
$d_{\rm lat} = 17$	
1.99×10^{-1}	2.32×10^{-3}
4.63×10^{-1}	1.83×10^{-4}
7.28×10^{-1}	1.97×10^{-5}
9.93×10^{-1}	2.34×10^{-6}
1.26	2.68×10^{-7}
1.52	3.97×10^{-8}
1.79	4.18×10^{-9}
2.05	4.68×10^{-10}
2.32	7.23×10^{-11}
2.58	8.65×10^{-12}
2.85	1.01×10^{-12}
3.11	1.28×10^{-13}
3.38	1.52×10^{-14}
3.64	1.43×10^{-15}
3.91	1.58×10^{-16}
4.17	2.09×10^{-17}
4.44	1.65×10^{-18}
4.7	1.55×10^{-19}
4.97	9.53×10^{-21}
5.23	7.83×10^{-22}
5.5	4.67×10^{-23}
5.76	1.60×10^{-24}
6.03	7.07×10^{-26}
6.29	1.84×10^{-27}
6.55	6.29×10^{-30}
$d_{\rm lat} = 21$	
2.07×10^{-1}	2.64×10^{-3}
4.65×10^{-1}	1.84×10^{-4}
7.23×10^{-1}	2.24×10^{-5}
9.81×10^{-1}	2.45×10^{-6}
1.24	3.30×10^{-7}
1.5	4.42×10^{-8}
1.76	4.79×10^{-9}
2.01	7.28×10^{-10}
2.27	9.43×10^{-11}
2.53	1.16×10^{-11}
2.79	1.83×10^{-12}
3.05	2.27×10^{-13}
3.31	2.49×10^{-14}
3.56	3.53×10^{-15}
3.82	4.55×10^{-16}
4.08	5.46×10^{-17}
4.34	6.83×10^{-18}
4.6	8.56×10^{-19}
4.86	9.23×10^{-20}
5.11	9.97×10^{-21}
5.37	9.97×10^{-22}
5.63	9.76×10^{-23}
5.89	8.84×10^{-24}
6.15	9.80×10^{-25}
6.41	7.34×10^{-26}
6.66	4.72×10^{-27}
6.92	2.69×10^{-28}
7.18	2.05×10^{-29}
7.44	1.02×10^{-30}
7.7	3.04×10^{-32}
7.96	1.37×10^{-33}
8.21	2.41×10^{-35}

$\bar{r}/d_{\rm avg}$	$\mathcal{N}$
$d_{\rm lat} = 25$	
2.18×10^{-1}	2.63×10^{-3}
4.79×10^{-1}	1.76×10^{-4}
7.41×10^{-1}	2.22×10^{-5}
1.	2.34×10^{-6}
1.26	3.34×10^{-7}
1.53	3.89×10^{-8}
1.79	5.17×10^{-9}
2.05	7.45×10^{-10}
2.31	8.57×10^{-11}
2.57	1.31×10^{-11}
2.83	1.83×10^{-12}
3.09	2.17×10^{-13}
3.36	3.20×10^{-14}
3.62	4.42×10^{-15}
3.88	5.13×10^{-16}
4.14	6.94×10^{-17}
4.4	9.14×10^{-18}
4.66	1.22×10^{-18}
4.93	1.47×10^{-19}
5.19	1.82×10^{-20}
5.45	2.03×10^{-21}
5.71	2.23×10^{-22}
5.97	2.60×10^{-23}
6.23	2.66×10^{-24}
6.49	2.93×10^{-25}
6.76	3.07×10^{-26}
7.02	2.89×10^{-27}
7.28	3.09×10^{-28}
7.54	2.26×10^{-29}
7.8	2.71×10^{-30}
8.06	2.19×10^{-31}
8.32	1.17×10^{-32}
8.59	6.11×10^{-34}
8.85	3.84×10^{-35}
9.11	2.11×10^{-36}
9.37	9.88×10^{-38}
9.63	4.29×10^{-39}
9.89	1.54×10^{-40}
1.02×10^{1}	3.35×10^{-43}

$\bar{r}/d_{\rm avg}$	$\mathcal{N}$
$d_{\rm lat} = 29$	
2.21×10^{-1}	2.80×10^{-3}
4.78×10^{-1}	1.92×10^{-4}
7.36×10^{-1}	2.34×10^{-5}
9.93×10^{-1}	2.60×10^{-6}
1.25	3.67×10^{-7}
1.51	4.23×10^{-8}
1.77	6.29×10^{-9}
2.02	8.45×10^{-10}
2.28	1.08×10^{-10}
2.54	1.67×10^{-11}
2.8	2.20×10^{-12}
3.05	3.02×10^{-13}
3.31	4.44×10^{-14}
3.57	5.79×10^{-15}
3.83	7.79×10^{-16}
4.08	1.10×10^{-16}
4.34	1.42×10^{-17}
4.6	1.93×10^{-18}
4.86	2.62×10^{-19}
5.11	3.32×10^{-20}
5.37	4.36×10^{-21}
5.63	5.82×10^{-22}
5.89	7.26×10^{-23}
6.14	9.13×10^{-24}
6.4	1.20×10^{-24}
6.66	1.50×10^{-25}
6.92	1.60×10^{-26}
$d_{\rm lat} = 33$	
2.25×10^{-1}	2.71×10^{-3}
4.82×10^{-1}	1.90×10^{-4}
7.39×10^{-1}	2.24×10^{-5}
9.97×10^{-1}	2.58×10^{-6}
1.25	3.47×10^{-7}
1.51	4.20×10^{-8}
1.77	6.28×10^{-9}
2.03	7.75×10^{-10}
2.28	1.10×10^{-10}
2.54	1.61×10^{-11}
2.8	2.08×10^{-12}
3.05	3.17×10^{-13}
3.31	4.37×10^{-14}
3.57	5.71×10^{-15}
3.83	8.27×10^{-16}
4.08	1.13×10^{-16}
4.34	1.53×10^{-17}
4.6	2.15×10^{-18}
4.85	2.87×10^{-19}
5.11	3.92×10^{-20}
5.37	5.28×10^{-21}
5.63	6.77×10^{-22}
5.88	8.52×10^{-23}
6.14	1.13×10^{-23}

TABLE S1. The numerically determined negativity between 3D pixelated spherical lattice regions as a function of normalized separation. The columns of finer-pixelation (d = 29, 33) do not show results throughout the entire range of non-vanishing negativity.

correlation functions at long distances to produce an exponentially decaying residual sensitive to the short-distance physics. Table S2 shows the results obtained for the radius of the negativity sphere for different region sizes using the improved lattice dispersion relations. The negativity between regions of different sizes are shown in Fig. S4 for two different dispersion relations. Away from the continuum limit, the negativity exhibits oscillations that depend upon the dispersion relation, and as such lead to fluctuations in the separability radius but do not change the scale setting the exponential dependence on separation. As discussed, the negativity at smaller separations is less sensitive to the high-momentum behavior, consistent with a smaller dependence on the dispersion relation improvement.

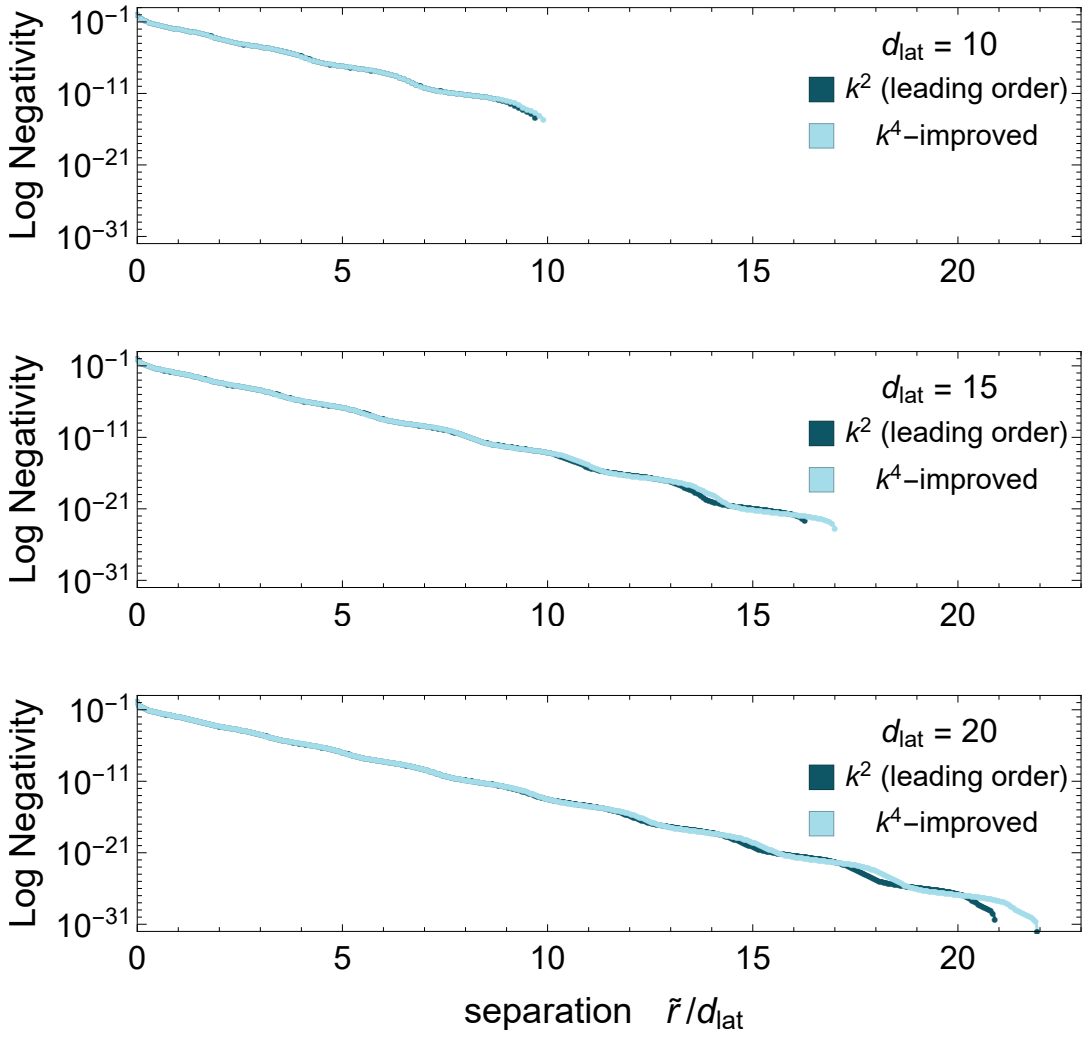

FIG. S4. The logarithmic negativity calculated with two different dispersion relations (k^2 leading order and k^4-improved) for one-dimensional region lengths of 10(top), 15(middle), and 20(bottom) lattice sites. Sensitivity to the UV modification appears at large spatial separation, as discussed in the main text.

k^2					
d_{lat}	$\tilde{r}_{\mathcal{N}}$	$\tilde{r}_{\mathcal{N}}/d_{lat}$			
1	1	1.00	11	131	11.90
2	2	1.00	12	144	12.00
3	9	3.00	13	184	14.20
4	13	3.25	14	199	14.20
5	26	5.20	15	245	16.30
6	32	5.33	16	264	16.50
7	52	7.43	17	316	18.60
8	61	7.63	18	337	18.70
9	87	9.67	19	395	20.80
10	98	9.80	20	419	21.00

k^4					
d_{lat}	$\tilde{r}_{\mathcal{N}}$	$\tilde{r}_{\mathcal{N}}/d_{lat}$			
1	1	1.00	11	135	12.30
2	2	1.00	12	148	12.30
3	9	3.00	13	190	14.60
4	12	3.00	14	207	14.80
5	26	5.20	15	256	17.10
6	32	5.33	16	275	17.20
7	53	7.57	17	331	19.50
8	61	7.63	18	352	19.60
9	89	9.89	19	415	21.80
10	100	10.00	20	440	22.00

TABLE S2. Negativity sphere radii for regions of the one-dimensional massless scalar field with a nearest neighbor lattice action (k^2) and order k^4-improvement of the dispersion relation.